Journal of Physics and Chemistry of Solids 169 (2022) 110872

Contents lists available at ScienceDirect

Journal of Physics and Chemistry of Solids

journal homepage: www.elsevier.com/locate/jpcs

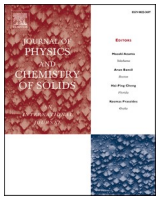

# The effect of growth potential on the self-discharge behavior of Cu–Ni based alloy electrodes

Abdulcabbar Yavuz [a,*], Murat Artan [b], Necip Fazil Yilmaz [b,c]

[a] Gaziantep University, Department of Metallurgical and Materials Engineering, Sehitkamil, 27310, Gaziantep, Turkey
[b] Gaziantep University, Department of Mechanical Engineering, Sehitkamil, 27310, Gaziantep, Turkey
[c] Hasan Kalyoncu University, Board of Trustees, 27010, Gaziantep, Turkey

ARTICLE INFO

*Keywords:*
Metal oxide
Supercapacitor
Ionic liquid
Graphite
Alloys
Self-discharge

ABSTRACT

Recently, the increasing demand for sustainable clean energy from non-fossil sources motivated the researchers in energy storage devices and supercapacitors are one of the most promising energy storage systems. In this study, flexible copper and nickel coated electrodes are fabricated for supercapacitor applications from Ethaline deep eutectic solvent media. Copper and nickel-based materials were potentiostatically electrodeposited on flexible graphite substrates from Ethaline ionic liquid containing copper and nickel ions. Cu–Ni coated graphite films were scanned in 1 M KOH from −0.7 V to 0.4 V at different scan rates ranging between 5 mV $s^{-1}$ and 100 mV $s^{-1}$. Fabricated Cu–Ni electrodes were characterized by scanning electron microscopy (SEM), Fourier transform infrared spectroscopy (FTIR) and X-ray diffraction (XRD). Copper and nickel formation ratios on graphite films at different deposition voltages were determined by EDX analysis. Cu–Ni coated graphite films applying −1.8 V deposition potential exhibited a maximum areal capacitance of 47.3 mF $cm^{-2}$ at 5 mV $s^{-1}$ scan rate. Galvanostatic charge-discharge curves of the electrodes obtained at different applied voltages confirms the supercapacitor behaviour of Cu–Ni coated films. One of the biggest issues regarding the use of supercapacitors in daily life is their self-discharge behaviour. Self-discharge curves of the Cu–Ni modified electrodes were illustrated that decreasing deposition potentials can decrease self-discharge problem. This research determines that Ethaline ionic liquid is a potential media for alloy-based electrodes in the usage of supercapacitor applications.

## 1. Introduction

The unintended and negative ecological impacts caused by the uncontrolled consumption of fossil fuels have raised serious concerns about developing sustainable and renewable energy production processes, as well as reviewing the phenomena of efficient storage and conversion [1]. In this case, electrochemical energy storage devices such as supercapacitors, batteries and fuel cells have made rapid advances to meet the increasing demands of non-stop energy supply [2]. To date, batteries are considered the main electrochemical energy storage systems due to their high energy densities [3]. However, low lifetime, low specific power, ecological pollution and safety issues related to end-of-life recycling and disposal are the most important practical limitations in the use of batteries [4]. However, the lack of energy storage systems that can replace existing batteries has been one of the main reasons for ignoring their disadvantages [5]. As an alternative to batteries, fuel cells based on hydrogen provide no $CO_2$ emissions and a favourable energy conversion rate but suffer from some disadvantages including their large size, insufficient fuel storage capacity and large installation costs [6]. Although conventional capacitors exhibit lower specific energy unlike others, they can provide energy at an extremely fast rate and have a long cycle life [7]. Thus, researchers began integrating all the cutting-edge features of all types of electrochemical energy storage systems to produce alternative energy storage devices with high energy-conducting capabilities in the form of supercapacitors, also called electrochemical capacitors or ultracapacitors [8]. However, the energy-power efficiency of supercapacitors is much lower than expected [9]. Therefore, instead of bulky, poorly responding and low cycle life batteries, it has become important to develop portable, small and bendable as well as strong and useful supercapacitors with high specific energy and power capabilities. A significant problem regarding the usage of supercapacitor in common applications such as hybrid cars and household items is the self-discharge of supercapacitor electrodes [10]. Therefore, numerous studies have been conducted to overcome the self-charge behaviour of

* Corresponding author.
*E-mail address:* ayavuz@gantep.edu.tr (A. Yavuz).

https://doi.org/10.1016/j.jpcs.2022.110872
Received 12 March 2022; Received in revised form 1 June 2022; Accepted 23 June 2022
Available online 27 June 2022

supercapacitor materials [11].

Compared to batteries, supercapacitors have a lower energy density so it is becoming more important to store energy in a fast, efficient and inexpensive way with high energy density. The capacitances of supercapacitor electrodes originate from the accumulation of charges at the electrode and electrolyte interaction [8]. One of the ways to obtain a high energy density is to increase the operating voltage window. The potential window of supercapacitor could be extended by using ionic liquids [12, 13]. In addition, ionic liquid electrolytes started to be used in energy storage systems not only because of their wide potential window but also they have non-flammable behaviour, stable electrochemical characteristics and low vapour pressure [14].

Supercapacitors have a wide range of applications where storing and releasing energy rapidly. Recently, supercapacitors have been studied to increase the efficiency and performance for using them in hybrid electric and fuel cell vehicles such as passenger cars, trolleybuses, trains, flexible and portable electronic devices, personal computers, wind turbines and solar arrays [15, 16, 17]. For instance, supercapacitor practices in the automotive industry can have benefits as hybrid electric vehicles use energy stored in supercapacitors in order to efficiently start and stop their engine [2]. Starting a car requires a high demand of energy and rapid energy release of supercapacitors supply this energy to the system and decrease the energy consumption of the battery [18].

A supercapacitor cell consists of two electrodes with a separating material between them. These two electrodes are the same for symmetrical cells but differ from each other for asymmetrical cells [19]. The separator material is ion-permeable in order to provide ionic charge transfer, and it is immersed in an electrolyte to cut the electrical contact between the electrodes [20]. The types of supercapacitors can be divided into three main categories according to the energy storage mechanisms between electrodes and the electrolyte; these are pseudo-capacitors, electric double-layer capacitors (EDLCs) and hybrid capacitors [21]. EDLCs are based on the electrostatic interaction between the electrolyte and the surface of the electrodes and EDLC electrodes with high surface are preferred [13]. Activated carbon, carbon nanotubes and graphene are most widely used materials in EDLC electrodes because they could have nanoporous surfaces and these materials are produced already in the industry [17]. Pseudocapacitors store energy by a mechanism based on rapid redox reactions occurring on the surface of the electrodes, and electrode materials are commonly produced using metal oxides and conductive polymers, and the specific capacitance values of these materials could be as high as that of EDLCs' materials [22]. Finally, hybrid electrodes could consist of a pseudocapacitive and an EDLC electrode, combining the features of both systems [23]. The negative and positive electrode of the hybrid capacitor could made from a pseudocapacitive electrode material having redox reactions or a carbon material storing the energy electrostatically. This interaction between the electrolyte and the surface of the electrode may provide a high delivery of currents. Hybrid supercapacitors are not commercially available and a typical example of hybrid systems is a lithium-ion capacitor [24, 25].

Electrode materials are one of the most fundamental factors for supercapacitors and can typically be divided into three distinct groups as carbon materials, conductive polymers, and metal oxides [26]. The low cost, well developed surface area, chemical stability, and good electrical conductivity of carbon materials make them ideal materials for EDLCs, but they generally suffer from relatively low specific capacitance [27, 28]. Conductive polymers could have higher specific capacitance than carbon materials, but their cycle life is extremely lower than EDLCs [29, 30]. Compared to these two types of materials, metal oxides usually have fast redox reaction states, which allows them to have higher specific capacitance [22]. They also have been regarded as promising supercapacitor electrode materials for energy storage devices because of their abundance, environmental friendliness and easy accessibility [31]. Various types of metal oxides have been analysed in pseudocapacitors in literature such as manganese [32], iron [33], nickel [34], ruthenium [35], copper [36], tin [37], cobalt [38], tungsten [39], vanadium [40], molybdenum [41] and lead [42] based oxides/hydroxides.

The self-discharge is a problem related with the energy loss of the energy storage devices due to the rapid drop of the voltage and an undesired and harmful characteristic for supercapacitors. It is one of the main problems for the practical applications of supercapacitors and efforts to suppress self-discharge rate to minimum is an issue among the researchers. Although the self-discharge phenomena cannot be completely eliminated, it can be suppressed to the lowest point. Several approaches have been tested to achieve this purpose. All components of supercapacitors were examined (studied) to suppress the self-discharge. The electrodes (both positive and negative) have been modified, the electrolytes have been modulated and the separators have been tuned. There are numerous influences examined regarding self-discharge rates. Increasing leakage current according to the impurities in the electrolyte [43], effect of reducing viscosity by application of high operating temperatures [44], high charge current density effecting to have not enough time to form a stable electric double layer [44], weak interaction between the ions in the electrolyte and the surface of the electrode because of the oxygen groups [45], charge redistribution on the porous structure of electrode materials [46] are some of the investigated reasons which may affect the self-discharge.

Three main aspects to suppress the self-discharge behaviour of supercapacitors are the modification of the electrode materials, modulation of the electrolyte and regulating the separator. By modifying the electrode material, the reasons to bring about the self-discharge including the leakage current, dissolved oxygen in electrolyte and charge redistribution may be suppressed [45, 47–53]. Electrolyte also affects the self-discharge behaviour of supercapacitors by its viscosity and ion size. There are numerous studies related with the electrolyte to overwhelm the self-discharge problems [54–60]. Positive and negative electrodes can be insulated with a separator membrane to affect the movement of electrolyte ions, resulting the inhibition of shuttle effects. This is one of the useful strategy to overcome the self-discharge problem [61, 62]. In this study, the self-discharge behavior of the electrode was examined depending on the growth conditions of the electrode electrodeposited from an ionic liquid media.

Few studies have investigated the behavior of electrochemically grown electrodes during self-discharge [63]. Molybdenum-based electrodes composed of agglomerated nanoparticles were grown by electrochemical deposition from an aqueous electrolyte on stainless steel current collector [64]. It was reported that improved low self-discharge behavior was observed upon increasing the film thickness of the Mo-based coating. $Ni(OH)_2$ was electrodeposited in an aqueous solution on carbon cloth having carbon nanotubes [65]. This electrode illustrated a better self-discharge rate when charging by optimal time and current density. A thin layer poly(p-phenylene oxide) was electrodeposited on a carbon-based substrate. Although this coating decreased the specific capacitance by ~56%, the self-discharge of the electrode was reduced by 78% [50]. Tellurium nanorods electrosynthesized on carbon cloth for use in flexible energy storage devices displayed better self-discharge characteristics [66]. This is, as far as we know, the first study on the self-discharge of alloys electrodeposited from a non-aqueous ionic liquid electrolyte.

This study presents a stable and electroactive Cu–Ni alloyed electrode on flexible graphite substrates by application of different voltages using Ethaline ionic liquid. The growth conditions of the alloy were studied. Copper and nickel alloy films obtained by electrochemical deposition on graphite electrodes were investigated in potassium hydroxide (KOH) solution to test their supercapacitive performance. Surface characteristics, compositions and structure of the Cu–Ni coated films in case of different applied voltages were examined via scanning electron microscopy (SEM), X-ray powder diffraction (XRD), Energy Dispersive X-Ray Analysis (EDX) and Fourier transform infrared radiation spectrometry (FTIR).

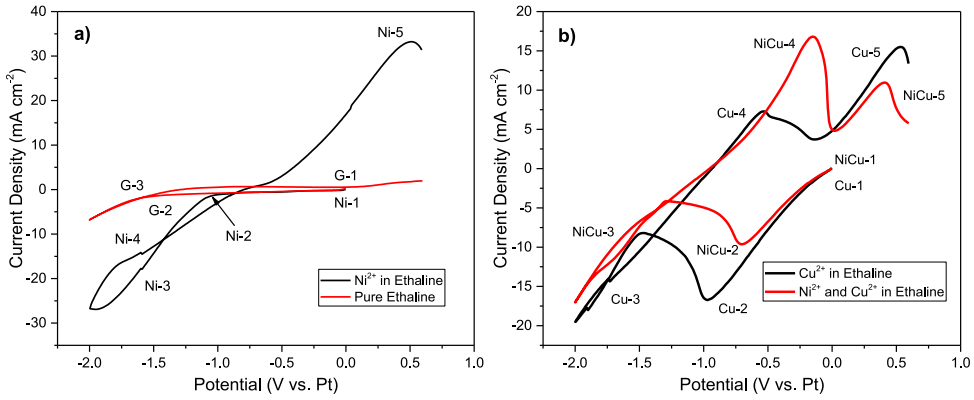


**Fig. 1.** Cyclic voltammetry curves of bare graphite electrode in a) pure Ethaline (red line) and 0.2 M $Ni^{2+}$ in Ethaline; b) 0.2 M $Cu^{2+}$ in Ethaline (black line) and Ethaline having the mixture of 0.1 M $Ni^{2+}$ and 0.1 M $Cu^{2+}$ (red line) at 65 °C at the scan rate of 50 mV $s^{-1}$

## 2. Methods

Copper (II) chloride ($CuCl_2$, Merck, ≥ 99%), nickel (II) chloride ($NiCl_2$, Merck, ≥ 98%), potassium hydroxide (KOH, Tekkim, ≥ 90%), ethylene glycol ($C_2H_6O_2$, Merck, ≥ 98%) and choline chloride ($C_5H_{14}ClNO$, Merck, ≥ 98%) were used as experimental chemicals in the study. Ethaline deep eutectic solvent was used as deposition medium which had been prepared by mixing and heating choline chloride and ethaline glycol in a 1:2 ratio at 65 °C until a liquid homogenous solution was acquired. 0.2 M $CuCl_2$ and 0.2 M $NiCl_2$ solutions were prepared in Ethaline ionic liquid by heating to 65 °C and mixing until dissolving completely. Copper and nickel-based solutions are then mixed to each other in 1:1 ratio and 0.1 M $CuCl_2$ with 0.1 M $NiCl_2$ deposition solution was prepared. Copper and nickel deposition was carried out on flexible graphite substrate which has a thickness of 1 mm. A three-electrode system was established using a platinum counter electrode and a wire platinum reference electrode. Copper and nickel mixed media was heated to 65 °C and Cu–Ni based alloy was potentiostatically electrodeposited on graphite substrate. Electrodeposition of the alloys on graphite electrodes were carried out by applying different voltages starting from −1.2 V to −1.8 V with 0.2 V interval for 600 s. Cu–Ni coated electrodes were immediately washed by pure water to refine from any impurities and then dried by hot air. Cycling experiments were conducted by using 1 M KOH media at room temperature by setting up a conventional three-electrode system. Counter electrode was again a platinum plate and reference electrode was an Ag–AgCl in saturated KCl while the working electrode was Cu–Ni coated flexible graphite electrodes. Cu–Ni coated electrodes were cycled in 1 M KOH between −0.7 V and 0.4 V (1.1 V potential window) at varying scan rates ranging from 5 mV $s^{-1}$ to 100 mV $s^{-1}$ in order to investigate the related electrochemical behaviour and performance. All conventional three-electrode experiments were carried out by AMETEK VersaSTAT potentiostat device. Galvanostatic charge-discharge and self-discharge experiments of the Cu–Ni coated films were performed in alkaline media by using a graphite fabric as opposite electrode. Charge-discharge and self-discharge graphs were obtained by Gamry 1010E device and overall data were analysed by Gamry Echem software. Absorption and emission spectra of the Cu–Ni alloy films were revealed by FTIR analysis (Perkin Elmer). Crystalline phases of the Cu–Ni alloy were obtained by XRD analysis (PANalytical Empyrean) and morphology of the films were elucidated using SEM and EDX (Zeiss Sigma) analysis.

## 3. Results and discussion

The proper voltage for nickel and copper electrodeposition on graphite was determined using the cyclic voltammetry method. Cyclic voltammetry is a widely used electrochemical method for detecting redox reactions at electrodes and/or electrolytes. The electrodeposition behaviour of nickel and copper were studied on the graphite electrode in Ethaline deep eutectic solvent. First, the graphite electrode was scanned in pure Ethaline in order to examine the potential window and it is presented in Fig. 1a. Bare graphite started cycling in pure ethaline from zero voltage (indicated as point G-1 in red line of Fig. 1a) and there is not any reduction peak until the voltage reaches up to −1.6 V. A reduction peak occurs at around −1.6 V, which was resulted because of the hydrogen evolution reaction [67]. As a second experiment, bare graphite electrode was immersed in Ethaline deep eutectic solvent containing 0.2 M $Ni^{+2}$ ions in order to observe the nickel formation as shown in black line of Fig. 1a. Graphite film was started cycling from zero (given as Ni-1) which was near the open circuit potential to −2.0 V and then finished at +0.6 V at a scan rate of 50 mV $s^{-1}$ at 65 °C. A reduction peak starts occurring at around −1.0 V (indicated as Ni-2) which was related to the nickel grown on graphite film [68]. Reduction continue to decrease at more negative potential which is also related to nickel growth [68, 69]. The decrease of current value may also be related to hydrogen evolution reaction, which was clearly seen in graphite film curve in pure Ethaline. The oxidation peak of nickel ions was at around 0.5 V which is shown at point Ni-5 in Fig. 1a. Cyclic voltammogram of copper on graphite film was examined in Ethaline containing 0.2 M $Cu^{+2}$ at the scan rate of 50 mV $s^{-1}$ at 65 °C and the resulting curve is shown in black line of Fig. 1b. $Cu^{+2}$ ions shows two different reduction processes, one of them is starting at around −0.25 V, which is the formation of $Cu^{+}$ ions from $Cu^{2+}$ and the other starts at around −1.5 V, which is the reduction of $Cu^{+}$ ions to the metallic Cu. Stripping of copper from graphite starts at around −1.0 V which can be related with the oxidation of Cu to $Cu^{+}$ ions. An oxidation peak was observed at around +0.5 V, which is associated with $Cu^{+}$ ions to $Cu^{+2}$ [70, 71]. Cycling of graphite electrode was finally carried out in Ethaline containing both 0.1 M $Ni^{+2}$ and 0.1 M $Cu^{+2}$ ions. Cyclic curves of the mixture were obtained at 65 °C and at a scan rate of 50 mV $s^{-1}$ and the resulting curve was shown as a red line of Fig. 1b. Nickel and copper mixture in Ethaline ionic liquid exhibits similar pattern like only copper ions in Ethaline because the deposition was probably dominated by copper reduction which can be proved by EDS analysis. Red line of Fig. 1b shows that the reduction of alloys or only copper can occur after −1.0 V. Therefore, the deposition voltage was selected as the potentials less than −1.2 V in order to observe the elemental ratio of copper and nickel in the alloy. Cu–Ni based alloys were potentiostatically obtained by the application of −1.2 V, −1.4 V, −1.6 V and −1.8 V in order to investigate the effect of growth potential on electrochemical performance of the resulting films.

The morphological characteristics of the electrodeposited Cu–Ni alloy electrodes on graphite substrates were investigated by scanning electron microscope (SEM) and the images of the bare graphite and all of

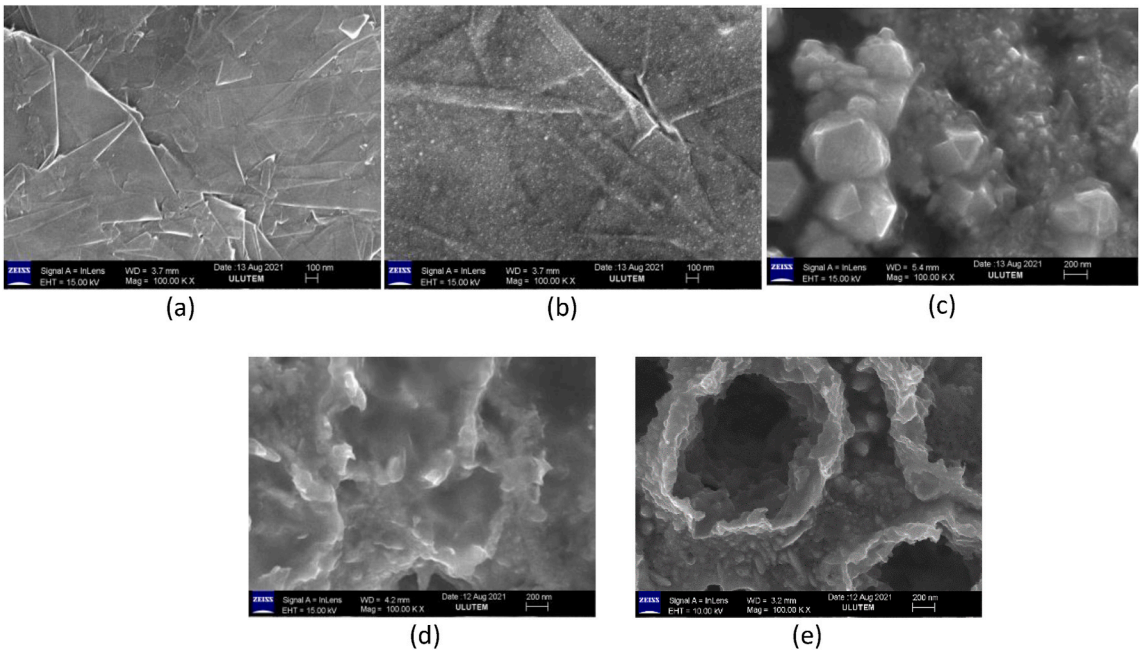


**Fig. 2.** SEM images of (a) bare graphite and Cu–Ni films electrodeposited from Ethaline media containing 0.1 M $Cu^{+2}$ and 0.1 M $Ni^{+2}$ ions by applying the constant potentials of (b) −1.2 V (c) −1.4 V (d) −1.6 V and (e) −1.8 V.

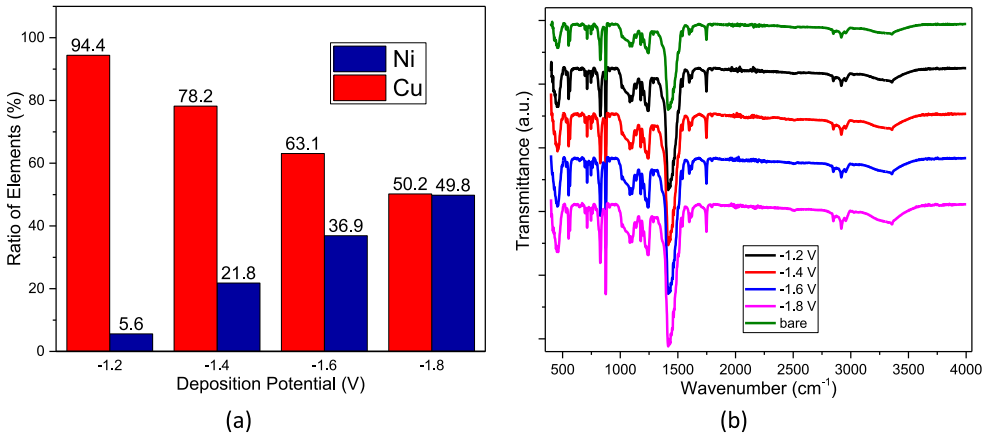


**Fig. 3.** a) EDX analysis result of the Cu–Ni coated films given in Fig. 2. b) FTIR results of bare graphite and Ni–Cu electrodeposited on the graphite film by the application of different deposition (growth potentials are indicated in the figure).

the obtained Cu–Ni alloy nanoparticles at nano level scales are shown in Fig. 2. Cu–Ni alloy film electrodeposited at −1.2 V in Ethaline ionic liquid has a slight coating (Fig. 2b) compared with the smooth multi-layer surfaces of bare graphite film (Fig. 2a). When the deposition potential was −1.4 V, strong agglomerations of the particles were observed on the Cu–Ni coated film and the size of the Cu–Ni alloy nanoparticles were varied (from tens of nanometers to micrometers). Surface structure of the Cu–Ni alloy was different when the film was electrodeposited by the application of lower potentials (Fig. 2d and e). Cu–Ni modified electrodes obtained by the −1.6 V and −1.8 V deposition potential from ionic liquid media have non-homogenous agglomerated nanoparticles. It is known that the nucleation mechanisms of the electrodeposition of metal could be different depending on pH [72], applied potential [73], additives [74], electrolyte temperature [75] and electrodeposition parameters [76]. Nucleation mechanism could cause various surface morphologies and grain or crystal sizes [77]. Additionally, hydrogen evolution reaction (depending on cathodic potential during metal/alloy growth) could affect surface morphology of the coating [78]. For example, intense hydrogen bubbling observed at more negative potential could change dense-branching of metal to fern-shaped dendrite of it [79]. Therefore, the lower potential (more negative voltage) applied to obtain Cu–Ni based film could have caused more porous nanostructures of the coating.

SEM analysis were used with the EDX mapping of the Cu–Ni coated films. Fig. 3a is the illustration of EDX mapping of the Cu–Ni alloy films on graphite substrate obtained at different deposition potentials. At −1.2 V deposition potential, almost the entire alloy consists of copper, while nickel has a slight composition ratio. Deposition potentials at −1.4 V and −1.6 V, nickel ratio gradually increases and reaches almost the same composition ratios as copper at −1.8 V. The results indicate that decreasing the deposition potential increases the nickel ratio and the decreases the copper ratio of the alloy coatings. A reduction of nickel was observed at around −1.0 V (indicated as Ni-2) [68] and the Ni growth continued to decrease at more negative potential [68, 69]. However, most of $Cu^{+2}$ was firstly reduced to $Cu^{+}$ at around −0.25 V and then significantly reduced to metalic copper at around −1.5 V [70, 71]. Fig. 1b displays that the cyclic voltammogram of nickel and copper mixture in Ethaline ionic liquid exhibits similar cyclic voltammogram

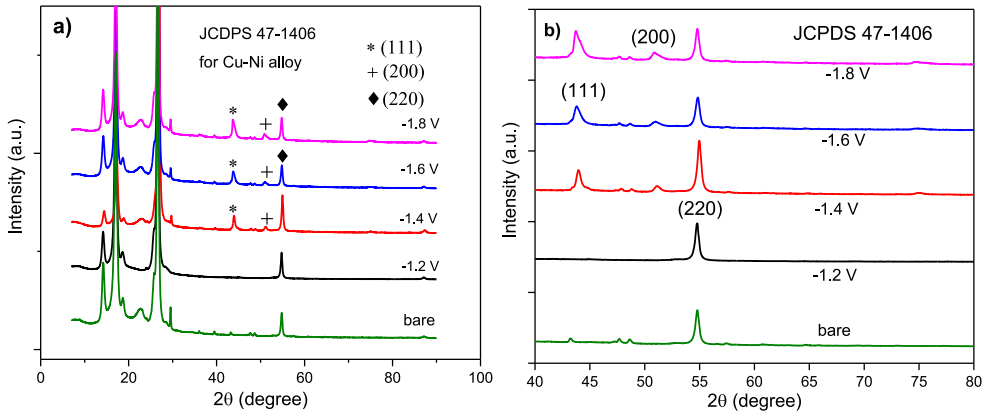


**Fig. 4.** a) XRD spectra of the Ni–Cu coatings on graphite film obtained at different deposition potentials. b) Detailed illustration of the peaks shown in panel a in order to observe the peaks clearly.

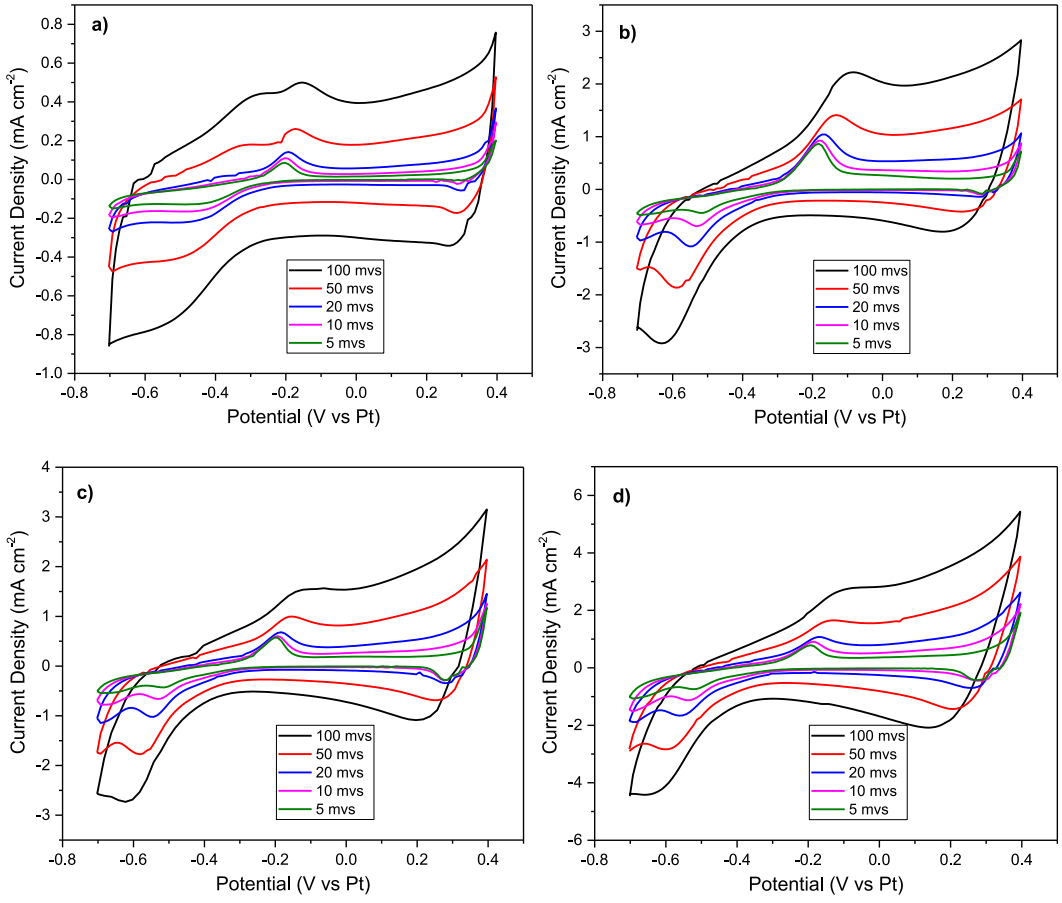


**Fig. 5.** Cyclic voltammograms of Ni–Cu alloy electrodes on graphite film cycled in 1 M KOH solution at the scan rates of 5, 10, 20, 50 and 100 mV $s^{-1}$. Electrodeposition potentials of the films are a) −1.2 V; b) −1.4 V; c) −1.6 V and; d) −1.8 V.

pattern like only copper ions in Ethaline. In Fig. 1, it can be seen that nickel ions in Ethaline starts reduction at around −1.0 V and continue its reduction at lower potentials. Additionally, copper ions in Ethaline begins to reduce at around −0.25 V and starts its evolution from $Cu^{+}$ ions to the metallic Cu at about −1.5 V. As the reduction potentials continue to decrease, reduction of the nickel and copper ions from Ethaline ionic liquid increases, growth of the alloy and agglomerations of the particles become intense at lower potentials.

Fig. 3b illustrates the FTIR graph of electrochemically deposited copper and nickel alloy thin films on the graphite substrate. The FTIR spectrum belonging to graphite had stretching vibrations of –OH peak at around 3410 $cm^{-1}$ and vibration of C═C group at 1610 $cm^{-1}$ due to $sp^2$ carbon atoms [80]. The spectrum also displays the C═O stretching at around 1750 $cm^{-1}$ [81] and the C–O stretching vibration at 1100 [82] due to probably purity in graphite [83]. Similar FTIR spectrum of graphite was observed in the literature [84,85]. From the FTIR spectrum, there is not a significant absorption peak related with the copper and nickel based oxide or hydroxide since the bare graphite film and Cu–Ni coated electrodes have the same absorption peaks [86,87]. This indicates that copper and nickel were probably electrodeposited on

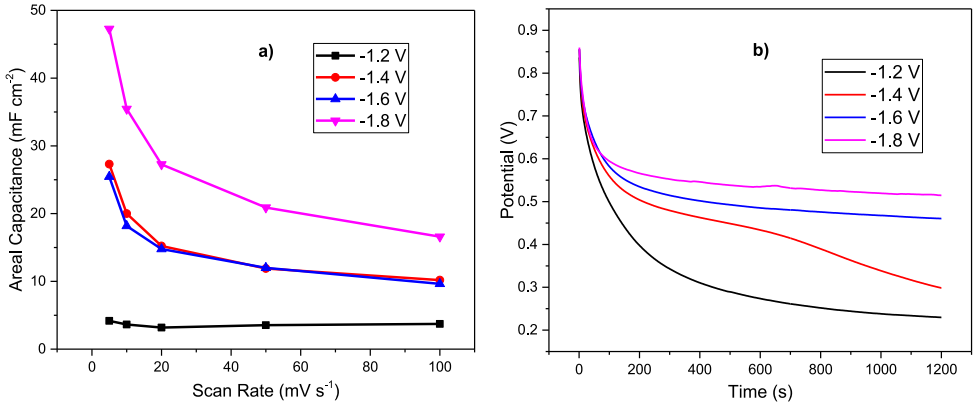


**Fig. 6.** a) Areal capacitances of the films against the scan rates. The values were calculated using Equation (1) and raw data in Fig. 5. b) The curves of self-discharge performance belonging to Cu–Ni coated electrodes electrodeposited at constant voltages indicated in the figure.

graphite as alloys (not their oxide or hydroxide forms).

Since the FTIR analysis did not provide enough information about the formation of copper and nickel on graphite film, a further analysis by XRD was carried out in order to elucidate the growth of metals on graphite substrate by electrodeposition from Ethaline ionic liquid. Fig. 4 depicts the XRD pattern of electrochemically deposited Cu–Ni alloys on graphite film. It can be observed from the XRD pattern that there are three major peaks related to nickel and copper metals/alloys. In order to observe these related peaks clearly, magnified curves of the XRD peaks based on copper and nickel coatings are illustrated in Fig. 4b. The XRD results of electrode formed at −1.2 V on graphite was similar to that of bare graphite because of slight deposition of the film. The diffraction peaks obtained from electrodes electrodeposited at −1.4 V, −1.6 V and −1.8 V appeared near 44°, 51° and 74.5° were the characteristics of (111), (200) and (220) copper-nickel alloy which was corresponded well with the peaks in JCPDS 47–1406 [88, 89]. XRD analysis proves the formation of copper and nickel alloys obtained on graphite electrode from Ethaline ionic liquid.

Characterization of the Cu–Ni alloy films are carried out by SEM, EDX, FTIR and XRD analysis and presented above. To understand the electrochemical behaviour of the Cu–Ni alloys on graphite, cyclic voltammogram curves are obtained by scanning the Cu–Ni based films in 1 M KOH electrolyte between −0.7 V and 0.4 V at the scan rates of 5, 10, 20, 50 and 100 mV s$^{-1}$. Cyclic voltammogram of the alloy-based films are illustrated in Fig. 5. The curves display that the cyclic voltammogram of Cu–Ni coated films electrodeposited between −1.2 V and −1.8 V depicts a nearly similar shape and behaviour. All of the Cu–Ni coated electrodes have an increasing areal shape as the scan rate increases.

The areal capacitance values of the Cu–Ni alloy electrodes obtained by applying different voltages from −1.2 V to −1.8 V in Ethaline ionic liquid media are presented in Fig. 6a. The areal capacitance of the films was found by using raw data of cyclic voltammogram curves illustrated in Fig. 5. Areal capacitances of the Cu–Ni alloy electrodes were calculated from the following equation [90,91]:

$$C_p = \frac{1}{A\, v\, \Delta V} \int_{v_1}^{v_2} I\,(V) dV \qquad \text{Equation 1}$$

In which A is the area of the Cu–Ni film (1 cm$^2$), $v$ denotes the scanning rates (mV s$^{-1}$), $\Delta V$ is used for the potential window of the cyclic voltammogram and $I(V)dV$ represents the area of the oxidation curves shown in Fig. 5. Fig. 6a illustrates that Cu–Ni alloy films perform higher areal capacitance values when the electrodes were obtained at lower deposition voltages. Cu–Ni films electrodeposited at −1.4 V and −1.6 V exhibit nearly the same areal capacitances, while the highest areal capacitance values at different scan rates were obtained for the Cu–Ni alloy electrode electrodeposited at −1.8 V. Areal capacitance of Cu–Ni alloy films reaches its maximum value of 47.27 mF cm$^{-2}$ at 5 mV s$^{-1}$ scan rate for the film formed by applying −1.8 V electrodeposition voltage. Comparison of capacitances of the Cu and Ni based supercapacitor electrodes reported in the literature is presented in Table 1.

**Table 1**
Comparison of capacitances of the nickel and copper-based supercapacitor electrodes reported in the literature.

| Electrode Material | Method | Capacitance | Reference |
|---|---|---|---|
| NiO–$TiO_2$ | Potentiostatic anodization | 46.3 mF cm$^{-2}$ | [93] |
| $Ni(OH)_2$ | Facile hydrothermal | 35.67 mF cm$^{-2}$ | [94] |
| $Ni(OH)_2$ nanoboxes | Template-engaged route | 1689 F g$^{-1}$ | [95] |
| Porous nickel oxide | Ion transport | 28 F g$^{-1}$ | [96] |
| CuO | Sonochemical assisted | 158 F g$^{-1}$ | [97] |
| CuO/rGO | Hydrothermal | 80 F g$^{-1}$ | [98] |
| $Cu_2O$/CuO | Hydrothermal | 338 mF cm$^{-2}$ | [99] |
| Copper/nickel oxide composite | Electroplating | 296.2 F g$^{-1}$ | [100] |
| Ni–Cu foam | Electrodeposition | 105 F g$^{-1}$ | [101] |
| CuO nanosheets | Hydrothermal | 130.6 F g$^{-1}$ | [102] |
| Cu–Ni alloy | Eletrodeposition | 47.27 mF cm$^{-2}$ | This work |

Capacitors fail to store their full of charge slowly and their stored energy decrease in process of time. Self-discharge of supercapacitors states the ongoing decrease of the voltage, which occurs when a capacitor remained unconnected to a charging circuit. Self-discharge experiments were carried out in order to observe if a supercapacitor has a reliable resistance for capacitance leakages [11]. Higher value of the self-discharge resistance is expected for less capacitance leakages [92]. Fig. 6b demonstrates the self-discharge curves of the Cu–Ni coated electrodes electrodeposited at different constant voltages from −1.2 V to −1.8 V. Cu–Ni coated films were charged fully to 1 V for 2 min and all of them were left for self-discharging of 20 min. It is clearly observed from Fig. 6b that decreasing deposition voltages results in lower self-discharge performances. Almost half of the potential is retained constant for the Cu–Ni film electrodeposited at −1.8 V, which showed a worthy self-discharge performance. Self-discharge is an important criterion for supercapacitors and must be conducted because supercapacitors usually suffer from the self-discharge problem.

Galvanostatic charge and discharge (GCD) curves are mainly used to analyse if the electrode exhibits a capacitance or battery-like behaviour [103]. GCD results of the Cu–Ni alloy films obtained from Ethaline ionic liquid media are presented in Fig. 7. After the electrodeposition of Cu–Ni alloy films by applying constant potentials of −1.2 V, −1.4 V, −1.6 V and −1.8 V, GCD experiments of the samples were carried out at

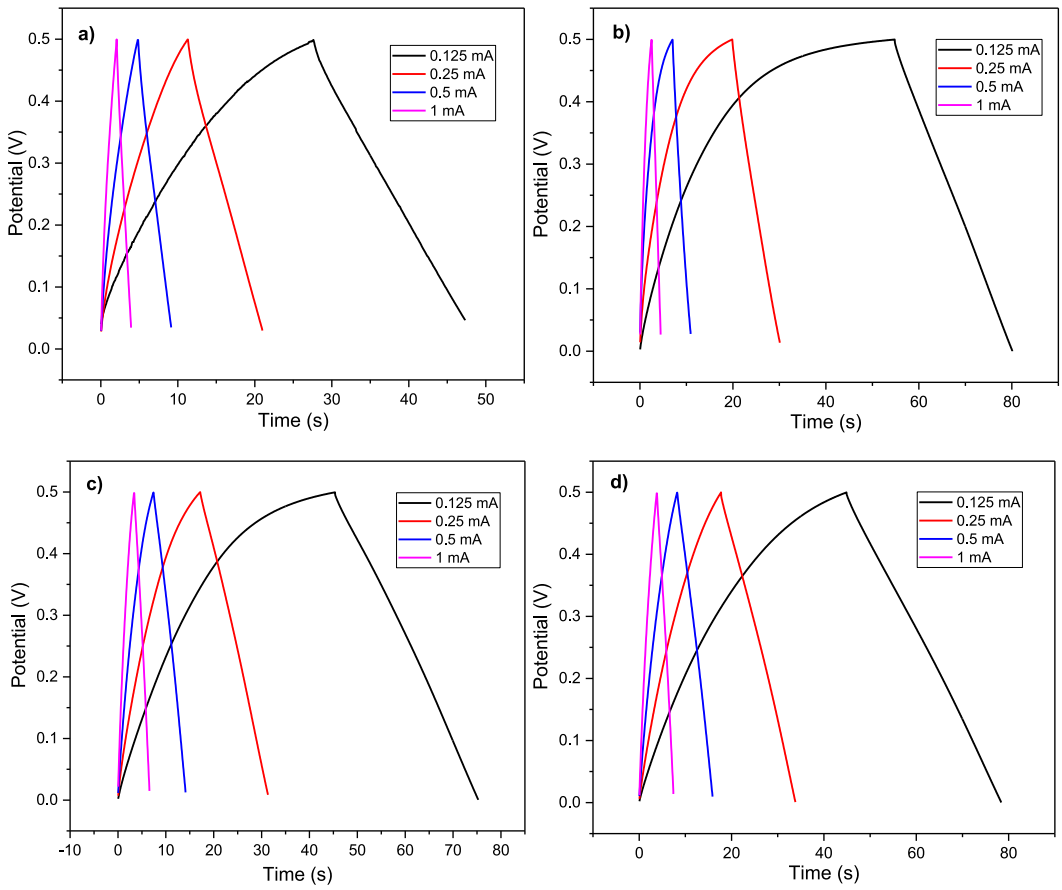


**Fig. 7.** Galvanostatic charge-discharge graph of Ni–Cu coated electrodes on graphite by applying different currents of 0.125 mA $cm^{-2}$, 0.25 mA $cm^{-2}$, 0.5 mA $cm^{-2}$ and 1 mA $cm^{-2}$. All coated electrodes were electrodeposited in Ethaline ionic liquid by applying different voltages of a) −1.2 V; b) −1.4 V; c) −1.6 V and; d) −1.8 V.

different constant currents per $cm^{-2}$ of 0.125 mA, 0.25 mA, 0.5 mA and 1 mA. All of the charge-discharge profiles exhibit nearly the similar triangle curves, which is the indicative of the typical supercapacitor behaviour [104, 105].

## 4. Conclusions

In summary, electrodeposition of copper and nickel was carried out on flexible graphite substrate by applying different constant voltages from Ethaline deep eutectic media containing 0.1 M $Cu^{+2}$ and 0.1 M $Ni^{+2}$ ions. SEM images of the Cu–Ni coated graphite films displayed the composition of copper and nickel alloy particles in nano structure. EDX mapping confirmed the deposition of copper and alloy by applying different constant potentials and decreasing the applied potentials resulted in an increase in the ratio of nickel and a decrease in the ratio of copper particles. Cu–Ni coated films were scanned in 1 M KOH electrolyte from −0.7 V to 0.4 V (1.1 V potential window) at different scan rates ranging between 5 mV $s^{-1}$ and 100 mV $s^{-1}$ in order to display the electrochemical behaviour and performance. Cu–Ni modified electrode electrodeposited at −1.8 V performed a maximum of 47.27 mF $cm^{-2}$ areal capacitance at 5 mV $s^{-1}$ scan rate. Decreasing deposition potentials of Cu–Ni alloy films increased the areal capacitance values but also the deposition potentials of −1.4 V and −1.6 V showed nearly the same areal capacitance performances. Charge-discharge curves in different applied currents performed the supercapacitor behaviour of the Cu–Ni alloy films by displaying a triangular-like shape. Self-discharge curves of the Cu–Ni alloy films showed a more stable self-discharge performance by the increase of applied deposition potential. As a result, copper and nickel alloy could be electrodeposited on graphite electrode from Ethaline ionic liquid by applying constant potentials to obtain inexpensive and easy-fabricated supercapacitor film.

## CRediT authorship contribution statement

Abdulcabbar Yavuz: Conceptualization, Formal analysis, Methodology, Data curation, Writing – review & editing, Supervision. Murat Artan: Methodology, Validation, Investigation, Writing – original draft. Necip Fazıl Yılmaz: Resources, Supervision, Writing – review & editing, Project administration, Funding acquisition.

## Declaration of competing interest

The authors declare that they have no known competing financial interests or personal relationships that could have appeared to influence the work reported in this paper.

## Acknowledgement

M.A. expresses his sincere thanks to YÖK for the PhD scholarship. The authors of this research also thank to Scientific Research Project Unit of Gaziantep University (MF.DT.20.13).

## References

[1] F. Barbir, T.N. Veziroğlu, H.J. Plass Jr., Environmental damage due to fossil fuels use, Int. J. Hydrogen Energy 15 (1990) 739–749.
[2] E. Karden, S. Ploumen, B. Fricke, T. Miller, K. Snyder, Energy storage devices for future hybrid electric vehicles, J. Power Sources 168 (2007) 2–11.
[3] A.K. Shukla, M.K. Ravikumar, T.S. Balasubramanian, Nickel/iron batteries, J. Power Sources 51 (1994) 29–36, https://doi.org/10.1016/0378-7753(94)01953-3.

[4] J. Xie, P. Yang, Y. Wang, T. Qi, Y. Lei, C.M. Li, Puzzles and confusions in supercapacitor and battery: theory and solutions, J. Power Sources 401 (2018) 213–223.

[5] J. Liu, J. Wang, C. Xu, H. Jiang, C. Li, L. Zhang, J. Lin, Z.X. Shen, Advanced energy storage devices: basic principles, analytical methods, and rational materials design, Adv. Sci. 5 (2018), 1700322.

[6] M.G. Carignano, R. Costa-Castelló, V. Roda, N.M. Nigro, S. Junco, D. Feroldi, Energy management strategy for fuel cell-supercapacitor hybrid vehicles based on prediction of energy demand, J. Power Sources 360 (2017) 419–433.

[7] R. Kötz, M. Carlen, Principles and applications of electrochemical capacitors, Electrochim. Acta 45 (2000) 2483–2498.

[8] J. Libich, J. Máca, J. Vondrák, O. Čech, M. Sedlaříková, Supercapacitors: properties and applications, J. Energy Storage 17 (2018) 224–227.

[9] B.E. Conway, Electrochemical Supercapacitors: Scientific Fundamentals and Technological Applications, Springer Science & Business Media, 2013.

[10] Y. Wang, X. Qiao, C. Zhang, X. Zhou, Self-discharge of a hybrid supercapacitor with incorporated galvanic cell components, Energy 159 (2018) 1035–1045, https://doi.org/10.1016/j.energy.2018.06.170.

[11] K. Liu, C. Yu, W. Guo, L. Ni, J. Yu, Y. Xie, Z. Wang, Y. Ren, J. Qiu, Recent research advances of self-discharge in supercapacitors: mechanisms and suppressing strategies, J. Energy Chem. 58 (2021) 94–109.

[12] J. Zhou, Z. Li, W. Xing, H. Shen, X. Bi, T. Zhu, Z. Qiu, S. Zhuo, A new approach to tuning carbon ultramicropore size at sub-angstrom level for maximizing specific capacitance and CO2 uptake, Adv. Funct. Mater. 26 (2016) 7955–7964.

[13] Y. Wu, J.-P. Cao, Q.-Q. Zhuang, X.-Y. Zhao, Z. Zhou, Y.-L. Wei, M. Zhao, H.-C. Bai, Biomass-derived three-dimensional hierarchical porous carbon network for symmetric supercapacitors with ultra-high energy density in ionic liquid electrolyte, Electrochim, Acta 371 (2021), 137825.

[14] S. Zhang, K. Dokko, M. Watanabe, Carbon materialization of ionic liquids: from solvents to materials, Mater. Horiz. 2 (2015) 168–197.

[15] L. Dong, C. Xu, Y. Li, Z.-H. Huang, F. Kang, Q.-H. Yang, X. Zhao, Flexible electrodes and supercapacitors for wearable energy storage: a review by category, J. Mater. Chem. A. 4 (2016) 4659–4685.

[16] R. Nigam, K.D. Verma, T. Pal, K.K. Kar, Applications of supercapacitors, in: Handb. Nanocomposite Supercapacitor Mater. II, Springer, 2020, pp. 463–481.

[17] W. Yang, M. Ni, X. Ren, Y. Tian, N. Li, Y. Su, X. Zhang, Graphene in supercapacitor applications, Curr. Opin. Colloid Interface Sci. 20 (2015) 416–428.

[18] Q. Xun, Y. Liu, X. Huang, E.A. Grunditz, J. Zhao, N. Zhao, Drive cycle energy efficiency of fuel cell/supercapacitor passive hybrid vehicle system, IEEE Trans. Ind. Appl. 57 (2020) 894–903.

[19] Y. Shao, M.F. El-Kady, J. Sun, Y. Li, Q. Zhang, M. Zhu, H. Wang, B. Dunn, R. B. Kaner, Design and mechanisms of asymmetric supercapacitors, Chem. Rev. 118 (2018) 9233–9280.

[20] Z. Wu, L. Li, J. Yan, X. Zhang, Materials design and system construction for conventional and new-concept supercapacitors, Adv. Sci. 4 (2017), 1600382.

[21] M. Vangari, T. Pryor, L. Jiang, Supercapacitors: review of materials and fabrication methods, J. Energy Eng. 139 (2013) 72–79.

[22] L. Zhou, C. Li, X. Liu, Y. Zhu, Y. Wu, T. van Ree, 7 - metal oxides in supercapacitors, in: Y.B.T. M.O, E.T. Wu (Eds.), Met. Oxides, Elsevier, 2018, pp. 169–203, https://doi.org/10.1016/B978-0-12-811167-3.00007-9, in.

[23] A. Muzaffar, M.B. Ahamed, K. Deshmukh, J. Thirumalai, A review on recent advances in hybrid supercapacitors: design, fabrication and applications, Renew. Sustain. Energy Rev. 101 (2019) 123–145, https://doi.org/10.1016/j.rser.2018.10.026.

[24] M. Park, Y. Lim, J. Kim, Y. Kim, J. Cho, J. Kim, A novel lithium-doping approach for an advanced lithium ion capacitor, Adv. Energy Mater. 1 (2011) 1002–1006.

[25] S. Li, J. Chen, M. Cui, G. Cai, J. Wang, P. Cui, X. Gong, P.S. Lee, A high-performance lithium-ion capacitor based on 2D nanosheet materials, Small 13 (2017), 1602893.

[26] P. Forouzandeh, V. Kumaravel, S.C. Pillai, Electrode materials for supercapacitors: a review of recent advances, Catalysts 10 (2020) 969.

[27] R. Dubey, V. Guruviah, Review of carbon-based electrode materials for supercapacitor energy storage, Ionics 25 (2019) 1419–1445.

[28] T. Chen, L. Dai, Carbon nanomaterials for high-performance supercapacitors, Mater. Today 16 (2013) 272–280.

[29] R. Ramya, R. Sivasubramanian, M. V Sangaranarayanan, Conducting polymers-based electrochemical supercapacitors—progress and prospects, Electrochim. Acta 101 (2013) 109–129.

[30] Y. Shi, L. Peng, Y. Ding, Y. Zhao, G. Yu, Nanostructured conductive polymers for advanced energy storage, Chem. Soc. Rev. 44 (2015) 6684–6696.

[31] F. Shi, L. Li, X. Wang, C. Gu, J. Tu, Metal oxide/hydroxide-based materials for supercapacitors, RSC Adv. 4 (2014) 41910–41921.

[32] M.N. Sakib, S. Ahmed, S.M.S.M. Rahat, S.B. Shuchi, A review of recent advances in manganese-based supercapacitors, J. Energy Storage 44 (2021), 103322.

[33] T. Eswaramoorthi, S. Ganesan, M. Marimuthu, K. Santhosh, Thin niobium and iron–graphene oxide composite metal–organic framework electrodes for high performance supercapacitors, New J. Chem. 44 (2020) 12664–12673.

[34] S.Y. Kim, T.Y. Yun, K.S. Yu, H.C. Moon, Reliable, high-performance electrochromic supercapacitors based on metal-doped nickel oxide, ACS Appl. Mater. Interfaces 12 (2020) 51978–51986.

[35] K. Brousse, S. Pinaud, S. Nguyen, P. Fazzini, R. Makarem, C. Josse, Y. Thimont, B. Chaudret, P. Taberna, M. Respaud, Facile and scalable preparation of ruthenium oxide-based flexible micro-supercapacitors, Adv. Energy Mater. 10 (2020), 1903136.

[36] Y. Bai, C. Liu, T. Chen, W. Li, S. Zheng, Y. Pi, Y. Luo, H. Pang, MXene-copper/cobalt hybrids via lewis acidic molten salts etching for high performance symmetric supercapacitors, Angew. Chem. 133 (2021) 25522–25526.

[37] Y.-H. Chan, C.-Y. Tsai, Y.-J. Shih, M.-S. Wu, Nanostructured tin oxide layer as a porous template for the growth of manganese oxide nanobouquets and a conductive support network for supercapacitors, Electrochim. Acta 364 (2020), 137329.

[38] S. Gayathri, P. Arunkumar, D. Saha, J.H. Han, Composition engineering of ZIF-derived cobalt phosphide/cobalt monoxide heterostructures for high-performance asymmetric supercapacitors, J. Colloid Interface Sci. 588 (2021) 557–570.

[39] A. De Adhikari, N. Shauloff, Y. Turkulets, I. Shalish, R. Jelinek, Tungsten-Disulfide/Polyaniline high frequency supercapacitors, Adv. Electron. Mater. (2021), 2100025.

[40] M.R. Pallavolu, Y.A. Kumar, R.R. Nallapureddy, H.R. Goli, A.N. Banerjee, S. W. Joo, In-situ design of porous vanadium nitride@ carbon nanobelts: a promising material for high-performance asymmetric supercapacitors, Appl. Surf. Sci. (2021), 151734.

[41] G.P. Awasthi, M.B. Poudel, M. Shin, K.P. Sharma, H.J. Kim, C. Yu, Facile synthesis of a copper oxide/molybdenum disulfide heterostructure for asymmetric supercapacitors of high specific energy, J. Energy Storage 42 (2021), 103140.

[42] S. Abraham, T. Prasankumar, K.V. Kumar, S.Z. Karazhanov, S. Jose, Novel lead dioxide intercalated polypyrrole/graphene oxide ternary composite for high throughput supercapacitors, Mater. Lett. 273 (2020), 127943.

[43] Q.D. Nguyen, Y.-H. Wu, T.-Y. Wu, M.-J. Deng, C.-H. Yang, J.-K. Chang, Gravimetric/volumetric capacitances, leakage current, and gas evolution of activated carbon supercapacitors, Electrochim. Acta 222 (2016) 1153–1159, https://doi.org/10.1016/j.electacta.2016.11.087.

[44] Q. Zhang, J. Rong, D. Ma, B. Wei, The governing self-discharge processes in activated carbon fabric-based supercapacitors with different organic electrolytes, Energy Environ. Sci. 4 (2011) 2152–2159.

[45] Y. Xie, W. Qiao, W. Zhang, G. Sun, L. Ling, Effect of the surface chemistry of activated carbon on its electrochemical properties in electric double layer capacitors, N. Carbon Mater. 25 (2010) 248–254, https://doi.org/10.1016/S1872-5805(09)60031-7.

[46] J.W. Graydon, M. Panjehshahi, D.W. Kirk, Charge redistribution and ionic mobility in the micropores of supercapacitors, J. Power Sources 245 (2014) 822–829, https://doi.org/10.1016/j.jpowsour.2013.07.036.

[47] Sutarsis, J. Patra, C.-Y. Su, J. Li, D. Bresser, S. Passerini, J.-K. Chang, Manipulation of nitrogen-heteroatom configuration for enhanced charge-storage performance and reliability of nanoporous carbon electrodes, ACS Appl. Mater. Interfaces 12 (2020) 32797–32805, https://doi.org/10.1021/acsami.0c08440.

[48] S. Yuan, X. Huang, H. Wang, L. Xie, J. Cheng, Q. Kong, G. Sun, C.-M. Chen, Structure evolution of oxygen removal from porous carbon for optimizing supercapacitor performance, J. Energy Chem. 51 (2020) 396–404, https://doi.org/10.1016/j.jechem.2020.04.004.

[49] A.M. Oickle, J. Tom, H.A. Andreas, Carbon oxidation and its influence on self-discharge in aqueous electrochemical capacitors, Carbon N. Y. 110 (2016) 232–242, https://doi.org/10.1016/j.carbon.2016.09.011.

[50] T. Tevi, H. Yaghoubi, J. Wang, A. Takshi, Application of poly (p-phenylene oxide) as blocking layer to reduce self-discharge in supercapacitors, J. Power Sources 241 (2013) 589–596, https://doi.org/10.1016/j.jpowsour.2013.04.150.

[51] J. Wang, B. Ding, X. Hao, Y. Xu, Y. Wang, L. Shen, H. Dou, X. Zhang, A modified molten-salt method to prepare graphene electrode with high capacitance and low self-discharge rate, Carbon N. Y. 102 (2016) 255–261, https://doi.org/10.1016/j.carbon.2016.02.047.

[52] Q. Zhang, C. Cai, J. Qin, B. Wei, Tunable self-discharge process of carbon nanotube based supercapacitors, Nano Energy 4 (2014) 14–22, https://doi.org/10.1016/j.nanoen.2013.12.005.

[53] C. Meng, C. Liu, L. Chen, C. Hu, S. Fan, Highly flexible and all-solid-state paperlike polymer supercapacitors, Nano Lett. 10 (2010) 4025–4031.

[54] A.M. Oickle, H.A. Andreas, Examination of water electrolysis and oxygen reduction as self-discharge mechanisms for carbon-based, aqueous electrolyte electrochemical capacitors, J. Phys. Chem. C 115 (2011) 4283–4288, https://doi.org/10.1021/jp1067439.

[55] Z. Wang, X. Chu, Z. Xu, H. Su, C. Yan, F. Liu, B. Gu, H. Huang, D. Xiong, H. Zhang, Extremely low self-discharge solid-state supercapacitors via the confinement effect of ion transfer, J. Mater. Chem. A. 7 (2019) 8633–8640.

[56] H. Avireddy, B.W. Byles, D. Pinto, J.M.D. Galindo, J.J. Biendicho, X. Wang, C. Flox, O. Crosnier, T. Brousse, E. Pomerantseva, Stable high-voltage aqueous pseudocapacitive energy storage device with slow self-discharge, Nano Energy 64 (2019), 103961.

[57] M. Xia, J. Nie, Z. Zhang, X. Lu, Z.L. Wang, Suppressing self-discharge of supercapacitors via electrorheological effect of liquid crystals, Nano Energy 47 (2018) 43–50, https://doi.org/10.1016/j.nanoen.2018.02.022.

[58] L. Chen, H. Bai, Z. Huang, L. Li, Mechanism investigation and suppression of self-discharge in active electrolyte enhanced supercapacitors, Energy Environ. Sci. 7 (2014) 1750–1759.

[59] H. Wang, J. Chen, R. Fan, Y. Wang, A flexible dual solid-stateelectrolyte supercapacitor with suppressed self-discharge and enhanced stability, Sustain. Energy Fuels 2 (2018) 2727–2732.

[60] S.-E. Chun, B. Evanko, X. Wang, D. Vonlanthen, X. Ji, G.D. Stucky, S. W. Boettcher, Design of aqueous redox-enhanced electrochemical capacitors with high specific energies and slow self-discharge, Nat. Commun. 6 (2015) 1–10.

[61] H. Peng, L. Xiao, K. Sun, G. Ma, G. Wei, Z. Lei, Preparation of a cheap and environmentally friendly separator by coaxial electrospinning toward suppressing

self-discharge of supercapacitors, J. Power Sources 435 (2019), 226800, https://doi.org/10.1016/j.jpowsour.2019.226800.
[62] H. Wang, Q. Zhou, B. Yao, H. Ma, M. Zhang, C. Li, G. Shi, Suppressing the self-discharge of supercapacitors by modifying separators with an ionic polyelectrolyte, Adv. Mater. Interfac. 5 (2018), 1701547.
[63] Y. Wu, R. Holze, Self-discharge in supercapacitors: causes, effects and therapies: an overview, Electrochem. Energy Technol. 7 (2021) 1–37.
[64] K.K. Upadhyay, T. Nguyen, T.M. Silva, M.J. Carmezim, M.F. Montemor, Electrodeposited MoOx films as negative electrode materials for redox supercapacitors, Electrochim. Acta 225 (2017) 19–28, https://doi.org/10.1016/j.electacta.2016.12.106.
[65] M.M. Ovhal, N. Kumar, S.-K. Hong, H.-W. Lee, J.-W. Kang, Asymmetric supercapacitor featuring carbon nanotubes and nickel hydroxide grown on carbon fabric: a study of self-discharging characteristics, J. Alloys Compd. 828 (2020), 154447, https://doi.org/10.1016/j.jallcom.2020.154447.
[66] S. Manoharan, K. Krishnamoorthy, V.K. Mariappan, D. Kesavan, S.-J. Kim, Electrochemical deposition of vertically aligned tellurium nanorods on flexible carbon cloth for wearable supercapacitors, Chem. Eng. J. 421 (2021), 129548, https://doi.org/10.1016/j.cej.2021.129548.
[67] M. Bučko, D. Culliton, A.J. Betts, J.B. Bajat, The electrochemical deposition of Zn–Mn coating from choline chloride–urea deep eutectic solvent, Trans. IMF. 95 (2017) 60–64.
[68] A.P. Abbott, K. El Ttaib, K.S. Ryder, E.L. Smith, Electrodeposition of nickel using eutectic based ionic liquids, Trans. IMF 86 (2008) 234–240.
[69] S. Wang, X. Zou, Y. Lu, S. Rao, X. Xie, Z. Pang, X. Lu, Q. Xu, Z. Zhou, Electrodeposition of nano-nickel in deep eutectic solvents for hydrogen evolution reaction in alkaline solution, Int. J. Hydrogen Energy (2018) 1–14, https://doi.org/10.1016/j.ijhydene.2018.06.188.
[70] P. Sebastian, E. Valles, E. Gómez, Copper electrodeposition in a deep eutectic solvent. First stages analysis considering Cu (I) stabilization in chloride media, Electrochim. Acta 123 (2014) 285–295.
[71] R. Bernasconi, M. Zebarjadi, L. Magagnin, Copper electrodeposition from a chloride free deep eutectic solvent, J. Electroanal. Chem. 758 (2015) 163–169.
[72] D. Grujicic, B. Pesic, Reaction and nucleation mechanisms of copper electrodeposition from ammoniacal solutions on vitreous carbon, Electrochim. Acta 50 (2005) 4426–4443, https://doi.org/10.1016/j.electacta.2005.02.012.
[73] A. Radisic, P.M. Vereecken, P.C. Searson, F.M. Ross, The morphology and nucleation kinetics of copper islands during electrodeposition, Surf. Sci. 600 (2006) 1817–1826, https://doi.org/10.1016/j.susc.2006.02.025.
[74] T. Otani, Y. Fukunaka, T. Homma, Effect of lead and tin additives on surface morphology evolution of electrodeposited zinc, Electrochim. Acta 242 (2017) 364–372, https://doi.org/10.1016/j.electacta.2017.04.130.
[75] A. Jabbar, G. Yasin, W.Q. Khan, M.Y. Anwar, R.M. Korai, M.N. Nizam, G. Muhyodin, Electrochemical deposition of nickel graphene composite coatings: effect of deposition temperature on its surface morphology and corrosion resistance, RSC Adv. 7 (2017) 31100–31109.
[76] F. Nasirpouri, M.R. Sanaeian, A.S. Samardak, E. V Sukovatitsina, A. V Ognev, L. A. Chebotkevich, M.-G. Hosseini, M. Abdolmaleki, An investigation on the effect of surface morphology and crystalline texture on corrosion behavior, structural and magnetic properties of electrodeposited nanocrystalline nickel films, Appl. Surf. Sci. 292 (2014) 795–805, https://doi.org/10.1016/j.apsusc.2013.12.053.
[77] S. Bijani, R. Schrebler, E.A. Dalchiele, M. Gabas, L. Martínez, J.R. Ramos-Barrado, Study of the nucleation and growth mechanisms in the electrodeposition of micro-and nanostructured Cu2O thin films, J. Phys. Chem. C 115 (2011) 21373–21382.
[78] V.S. Nikitin, T.N. Ostanina, V.M. Rudoi, T.S. Kuloshvili, A.B. Darintseva, Features of hydrogen evolution during electrodeposition of loose deposits of copper, nickel and zinc, J. Electroanal. Chem. 870 (2020), 114230, https://doi.org/10.1016/j.jelechem.2020.114230.
[79] P.-C. Hsu, S.-K. Seol, T.-N. Lo, C.-J. Liu, C.-L. Wang, C.-S. Lin, Y. Hwu, C.H. Chen, L.-W. Chang, J.H. Je, Hydrogen bubbles and the growth morphology of ramified zinc by electrodeposition, J. Electrochem. Soc. 155 (2008) D400.
[80] A. Hadi, J. Zahirifar, J. Karimi-Sabet, A. Dastbaz, Graphene nanosheets preparation using magnetic nanoparticle assisted liquid phase exfoliation of graphite: the coupled effect of ultrasound and wedging nanoparticles, Ultrason. Sonochem. 44 (2018) 204–214.
[81] S. Thakur, N. Karak, Green reduction of graphene oxide by aqueous phytoextracts, Carbon N. Y. 50 (2012) 5331–5339, https://doi.org/10.1016/j.carbon.2012.07.023.
[82] A.H. Wazir, I.W. Kundi, Synthesis of graphene nano sheets by the rapid reduction of electrochemically exfoliated graphene oxide induced by microwaves, J. Chem. Soc. Pakistan 38 (2016).
[83] C. Monteserín, M. Blanco, E. Aranzabe, A. Aranzabe, J.M. Laza, A. Larrañaga-Varga, J.L. Vilas, Effects of graphene oxide and chemically-reduced graphene oxide on the dynamic mechanical properties of epoxy amine composites, Polymers 9 (2017) 449.
[84] A.R. Fernandes, R.A. Bernardo, T.C. de Carvalho, B.G. Vaz, A.R. Chaves, Graphene oxides coated paper as a substrate to paper spray ionization mass spectrometry for creatinine determination in urine samples, J. Braz. Chem. Soc. 30 (2019) 1074–1081.
[85] E. Bulut, Electrochemically exfoliated graphene production by using different graphite sources, J. Turkish Chem. Soc. Sect. B Chem. Eng. 1 (2017) 149–158.
[86] P. Khanra, C.-N. Lee, T. Kuila, N.H. Kim, M.J. Park, J.H. Lee, 7, 7, 8, 8-Tetracyanoquinodimethane-assisted one-step electrochemical exfoliation of graphite and its performance as an electrode material, Nanoscale 6 (2014) 4864–4873.
[87] F.Y. Ban, S.R. Majid, N.M. Huang, H.N. Lim, Graphene oxide and its electrochemical performance, Int. J. Electrochem. Sci. 7 (2012) 4345–4351.
[88] Y. Huang, W. Xiang, R. Yang, L. Yan, X. Liang, Sol-gel derived glass nanocomposites embedded with phase-controlled Cu-Ni nanostructures and their optical nonlinearities, Mater. Lett. 189 (2017) 184–187.
[89] V. Zin, K. Brunelli, M. Dabalà, Characterization of Cu–Ni alloy electrodeposition and synthesis of nanoparticles by pulsed sonoelectrochemistry, Mater. Chem. Phys. 144 (2014) 272–279.
[90] Y.S.S. Sarma, N. Gupta, P. Bhattacharya, A composite electrode of 2D-Ti3C2 (MXene) and polyemeraldine salt of polyaniline for supercapacitor with high areal capacitance, Polym. Eng. Sci. 62 (6) (2022) 1918–1926. https://doi.org/10.1002/pen.25975.
[91] H. Zhou, G. Han, Y. Chang, D. Fu, Y. Xiao, Highly stable multi-wall carbon nanotubes@poly(3,4-ethylenedioxythiophene)/poly(styrene sulfonate) core–shell composites with three-dimensional porous nano-network for electrochemical capacitors, J. Power Sources 274 (2015) 229–236, https://doi.org/10.1016/j.jpowsour.2014.10.044.
[92] M. Haque, Q. Li, A.D. Smith, V. Kuzmenko, P. Rudquist, P. Lundgren, P. Enoksson, Self-discharge and leakage current mitigation of neutral aqueous-based supercapacitor by means of liquid crystal additive, J. Power Sources 453 (2020), 227897.
[93] Y. Xie, C. Huang, L. Zhou, Y. Liu, H. Huang, Supercapacitor application of nickel oxide–titania nanocomposites, Compos. Sci. Technol. 69 (2009) 2108–2114, https://doi.org/10.1016/j.compscitech.2009.01.018.
[94] X. Dong, Z. Guo, Y. Song, M. Hou, J. Wang, Y. Wang, Y. Xia, Flexible and wire-shaped micro-supercapacitor based on Ni (OH) 2-nanowire and ordered mesoporous carbon electrodes, Adv. Funct. Mater. 24 (2014) 3405–3412.
[95] Y. Fu, J. Song, Y. Zhu, C. Cao, High-performance supercapacitor electrode based on amorphous mesoporous Ni (OH) 2 nanoboxes, J. Power Sources 262 (2014) 344–348.
[96] D.-W. Wang, F. Li, H.-M. Cheng, Hierarchical porous nickel oxide and carbon as electrode materials for asymmetric supercapacitor, J. Power Sources 185 (2008) 1563–1568.
[97] A. Pendashteh, M.S. Rahmanifar, M.F. Mousavi, Morphologically controlled preparation of CuO nanostructures under ultrasound irradiation and their evaluation as pseudocapacitor materials, Ultrason. Sonochem. 21 (2014) 643–652, https://doi.org/10.1016/j.ultsonch.2013.08.009.
[98] I.Y.Y. Bu, R. Huang, Fabrication of CuO-decorated reduced graphene oxide nanosheets for supercapacitor applications, Ceram. Int. 43 (2017) 45–50, https://doi.org/10.1016/j.ceramint.2016.08.136.
[99] J.S. Chen, S.P. Huang, L. Xu, D.J. Blackwood, Sodium-Salt-promoted growth of self-supported copper oxides with comparative supercapacitive properties, Chemelectrochem 4 (2017) 3188–3195.
[100] J.L. Yin, J.Y. Park, Electrochemical investigation of copper/nickel oxide composites for supercapacitor applications, Int. J. Hydrogen Energy 39 (2014) 16562–16568, https://doi.org/10.1016/j.ijhydene.2014.04.202.
[101] S. Eugénio, T.M. Silva, M.J. Carmezim, R.G. Duarte, M.F. Montemor, Electrodeposition and characterization of nickel–copper metallic foams for application as electrodes for supercapacitors, J. Appl. Electrochem. 44 (2014) 455–465, https://doi.org/10.1007/s10800-013-0646-y.
[102] S.D. Jagadale, A.M. Teli, S. V Kalake, A.D. Sawant, A.A. Yadav, P.S. Patil, Functionalized crown ether assisted morphological tuning of CuO nanosheets for electrochemical supercapacitors, J. Electroanal. Chem. 816 (2018) 99–106, https://doi.org/10.1016/j.jelechem.2018.01.059.
[103] R. Ahmed, G. Nabi, Enhanced electrochemical performance of Cr-doped NiO nanorods for supercapacitor application, J. Energy Storage 33 (2021), 102115.
[104] W. Xing, C.C. Huang, S.P. Zhuo, X. Yuan, G.Q. Wang, D. Hulicova-Jurcakova, Z. F. Yan, G.Q. Lu, Hierarchical porous carbons with high performance for supercapacitor electrodes, Carbon N. Y. 47 (2009) 1715–1722.
[105] S. Devese, T. Nann, Suppressed self-discharge of an aqueous supercapacitor using Earth-abundant materials, J. Electroanal. Chem. 871 (2020), 114307.